A Numerical Study of Aircraft Wake Induced Ice Cloud Formation

K. M. GIERENS

DLR Oberpfaffenhofen, Institut für Physik der Atmosphäre, Weßling, Germany

J. STRÖM

Meteorologiska Institutionen, Stockholms Universitet, Stockholm, Sweden

(Manuscript received 27 January 1997, in final form 27 January 1998)

ABSTRACT

Numerical simulations of ice cloud formation in the wake of an aircraft flying at cruise altitude have been performed. The engine exhaust has been excluded from the simulations in order to study cloud formation due solely to aerodynamic effects. The ice is formed via homogeneous freezing nucleation of ambient haze droplets in the upwelling limbs of the vortex pair behind the aircraft. Properties of wake ice clouds are compared with properties of contrails obtained with in situ measurements and recent simulations. In particular, the authors find that aerodynamically induced ice clouds are similar in microphysical and radiative respects to contrails that are formed from the nucleation of exhaust particles. This means that under cold and moist conditions contrails as young as 2–5 min may consist of similar amounts of aerodynamically produced and exhaust triggered ice crystals.

1. Introduction

The potential for thin ice clouds to enhance the greenhouse effect (Stephens et al. 1990) has led to considerable interest regarding the anthropogenic perturbation on cirrus clouds caused by civil aviation. Estimates by Ponater et al. (1996) show that an increased cirrus cloud cover in the main global aircraft corridors of 2%–10% yield significant effects on atmospheric temperatures. This anthropogenic effect on cirrus clouds can be caused indirectly through altering formation processes due to an increased aerosol loading at cirrus altitudes from aircraft exhaust, or directly through the formation of a persistent cloud in the wake of an aircraft.

Appleman (1953) assumed that water saturation must be reached in the exhaust trail from an aircraft for a contrail to form. In order to reach water saturation in the plume, the ambient temperature must be below a certain critical value that depends on pressure, ambient humidity, and the ratio of water vapor and heat emission from the engine. However, there are some observations of contrails forming at temperatures above the Appleman threshold. For example, Sassen (1991) found a contrail below an altocumulus cloud where the conditions did not fulfill the Appleman criterion. Schumann (1996) took into account that some of the combustion heat is converted to work to propel the aircraft. This leads to threshold temperatures that are higher than those predicted by Appleman. The threshold temperature increases by 1.4 K for an increase of 0.1 in the propulsion efficiency.

Other situations where aircraft artificially produce large concentrations of ice crystals, not involving the exhaust, are termed aircraft produced ice particles (APIP). This phenomenon has been studied by several authors (e.g., Rangno and Hobbs 1983; Sassen 1991; Foster and Hallett 1993) and occurs when an aircraft moves through a supercooled cloud. The mechanisms thought to be responsible are splintering on leading surfaces and adiabatic cooling near the aircraft and propeller tips. This type of APIP is not likely to have a climatic impact but is of importance when making in situ measurements and reentering air already sampled. Nevertheless it is interesting to note that the mere disturbance of the air by the aircraft is able to form cloud particles. Such an effect can even be observed at ground, when cloud particles are formed at the wing tips of landing jets. The studies of APIP performed to date are limited to temperatures warmer than about -30°C. Commercial aircraft on the other hand, have their cruising altitudes mainly between 8 and 12 km, which corresponds to a temperature range between -30° and -60°C. Cloud formation at these temperatures is not yet fully understood, but an increasing number of studies (e.g., Sassen and Dodd 1989; Heymsfield and Miloshevich 1993; Ström et al. 1997) supports the idea that the most important ice nucleation process is through

Corresponding author address: Dr. Klaus M. Gierens, Deutsches Zentrum für Luft- und Raumfahrt (DLR), Institut für Physik der Atmosphäre, Postfach 1116, D-82230 Weßling, Germany.
E-mail: klaus.gierens@dlr.de

freezing of haze droplets. This implies that clouds form from 75% to 99% water saturation even at very cold temperatures, which is equivalent to high ice supersaturation. At a temperature of −50°C and a RH of 85%, small haze droplets are in an atmosphere supersaturated with respect to an ice surface and subsaturated with respect to a water surface. Thus, is it possible that the turbulence alone from an aircraft flying through a metastable (with reference to humidity) atmosphere can form an APIP trail? The magnitude of the vertical air motion caused by the trailing vortices behind a big airliner can be on the order of meters per second, which results in very strong turbulence. If an air parcel in the wake of the aircraft is lifted to the point where the humidity is increased enough for homogeneous freezing to occur, a cloud would rapidly form. Modeling studies by Lin et al. (1997) show that an air parcel with a humidity near the deliquescent point of ammonium sulfate (82%) only need an uplift of less than 50 m for a substantial cirrus cloud to form. To test the hypothesis that it is possible for an aircraft to form a contrail by the aerodynamic effects from the aircraft alone we have modeled a situation where the initial data is taken from aircraft measurements performed on 21 March 1994 over southern Germany.

In a previous paper on simulations of persistent contrails (Gierens 1996), formation of contrails in an aerosol-free environment was studied. The ambient aerosol was not considered in order to make the interpretation of the results clearer. In this study we take up the other extreme, excluding the effects of the exhaust from the aircraft. By separating the problem in this way we hope to highlight the processes at play. The next logical step is of course to include both the ambient and the exhaust aerosol in the model. This, however, requires a more sophisticated model than is currently at hand, with spectrally resolved microphysics and chemistry.

In the following we first describe the background for initializing the model (section 2), then we give a digest of the model and present the results of the simulations (section 3). The findings are discussed in section 4 and summarized in section 5.

2. Background

Water vapor emitted by aircraft is very important for the formation of contrails but adds only marginally to the ice water content (IWC). After a few minutes the contribution is less than 0.5 mg m^{-3} due to the strong dilution of the plume. Since the available water must be shared by the huge number of ice crystals formed in contrails, the size of contrail ice crystals cannot be very large. Nevertheless, Knollenberg (1972) observed ice crystals falling out of a contrail generated in an area void of natural cirrus. As pointed out by Knollenberg, the average size of the crystals must have been larger than 100 μm to have an appreciable settling velocity.

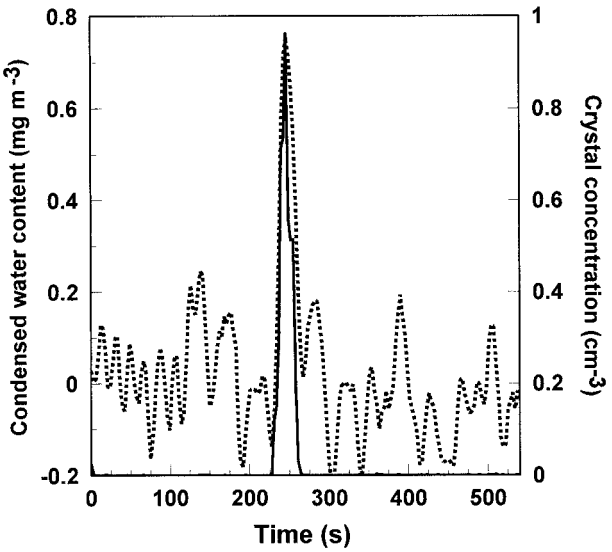

FIG. 1. Ice water content (dotted) and crystal concentration (solid) measured about 1000 m beneath a visible contrail in seemingly clear air.

Even if the available ambient water vapor were added, the contrail ice particles would not grow to large size.

If aerodynamic effects from aircraft are strong enough to form a contrail or cloud on ambient aerosols, without the exhaust being involved, this process could be a mechanism for growing a subset of crystals to precipitating sizes near contrails.

A more recent observation made with a counterflow virtual impactor (its principle of operation is described by Noone et al. 1988) also suggests precipitating particles associated with contrails. On 18 March 1994 an isolated peak in crystal concentration and IWC, presented in Fig. 1, was observed when the research aircraft Falcon passed perpendicularly under a visible contrail in otherwise cloud-free air. The vertical distance between the Falcon aircraft and the contrail was estimated to about 1 km. We have used the aerosol distribution observed on this day, approximated by two lognormal distributions (see below) to initialize the model.

For the atmospheric state variables we choose data obtained 21 March 1994. This was a day when many persistent contrails formed over southern Germany. In the measuring area the lower levels were almost overcast with stratocumulus clouds. At higher altitude, the wind was northerly and the sky almost clear except for occasional patches and streaks of visible cirrus clouds. To the north the cirrus clouds became more homogeneous, and to the south, over the Alps, the sky was completely free of clouds. In Figs. 2a and 2b, photographs taken on 21 March are presented to illustrate the situation on that day. Figure 2a shows a situation during a chase of a fresh (about 2 minutes old) contrail. Figure 2b shows an intersection of several aged contrails that merge together.

FIG. 2. Two photographs of the southern Germany sky of 21 March 1994, showing (a) a 2-min old contrail, and (b) a field of old expanded contrails that merge.

3. Simulations

a. The model

We employed the hydrodynamics software code MESOSCOP (Schumann et al. 1987) for the simulations. This code is supplemented with a cloud microphysics module, originally written by Höller (1986), and adapted for use in contrail simulations by Gierens (1996). For details of the code the reader is referred to the cited references.

The code uses a bulk formulation of the cloud microphysics. The prognostic variables are water vapor, IWC, number density of ice crystals, and number density of two types of aerosols (A and B). We assume that the masses of the ice crystals and the sizes of the aerosol particles obey a lognormal distribution in every cell of the computational grid. Geometric mean radius r_g and geometric standard deviation σ are prescribed for both aerosol types: for type A (small mode), $r_g = 0.05$ μm, $\sigma = 1.65$; for type B (large mode), $r_g = 0.3625$ μm, $\sigma = 1.4$. The mean mass of the ice crystals is given as the ratio of IWC and the crystal number density. The width of the ice crystal mass distribution is assumed to be proportional to the mean mass.

Microphysical processes that occur in the simulations are homogeneous freezing nucleation involving the aerosol particles and diffusional growth or evaporation of the ice crystals. Although coagulation is not switched off, it does not occur because at the low temperatures in contrail altitudes the sticking probability of colliding ice crystals is very low (e.g. Rogers, 1979), and furthermore the crystals remain small in the simulations (about 15 μm) so that the hydrodynamic drag (Kajikawa and Heymsfield, 1989) is not efficient. For the same reason, sedimentation is not important, although it is not switched off in the code. The growth and evaporation of the ice crystals is treated as in Gierens (1996); that is, we employ the Koenig (1971) type parametrization $\dot{m} = am^b$. For the formulation of the homogeneous freezing nucleation we use the method described by DeMott et al. (1994); details are given in the appendix.

All the simulations take place in a 2D 2 km $\times$ 2 km domain with a 20 m $\times$ 20 m grid. The simulation duration is 600 s with a time step of 2.5 s. The simulations are initialized with constant number densities of the aerosol particles: $\mathcal{N}_A = 500 \times 10^6$ m^{-3} for type A and $\mathcal{N}_B = 1 \times 10^6$ m^{-3} for type B. The relative humidity

is set constant to 85% in the beginning, which is just above the lower boundary of 82% for the ice formation parametrization of DeMott et al. (1994). There is no ice at the beginning of the simulations. A slightly stable temperature profile is prescribed with a nearly constant lapse rate of -8 K km^{-1}, which corresponds to a Brunt–Väisälä frequency of 9.5×10^{-3} s^{-1} or an oscillation period, T_{BV}, of about 11 min. Temperature and pressure in the aircraft cruise altitude are -56°C and 280 hPa. With these ambient conditions an exhaust contrail would form according to the Appleman criterion, which is also shown in Figure 2a. However, as stated before, we simply assume the engines to be switched off in order to isolate the aerodynamic contrail formation. An initial velocity field that is thought to be a result of the roll-up of the wingtip vortices shed from the aircraft wings has been implemented as follows: First we have prescribed a downward velocity of -2.5 m s^{-1} for a circular region of about 3×10^4 m^2 in the center of the computation domain. This solid-body motion does not satisfy the continuity equation. Thus, before the simulation begins the model calculates a new initial velocity field that satisfies the continuity equation (see Schumann et al. 1987, their appendix B). The result is a pair of counter-rotating vortices, the desired effect (cf. Gierens 1996). The pair of vortices is a source of turbulence in the otherwise calm background atmosphere. In the resulting complex flow field we have adiabatic heating and cooling. The cooling can trigger homogeneous freezing nucleation, that is, cloud formation.

Four cases have been considered: In case A we have only the small aerosol mode (type A), in case B there is only the large aerosol mode (type B). In case C we have assumed both aerosol modes to be present. Case D is a control run with both types of aerosols but without aircraft induced vortices. In this case the atmosphere is at rest and we can compare its results with those of case C in order to see the effect of the turbulent flow field on the ice formation. In neither case have we assumed background turbulence in order not to blur the effects of the aircraft-induced turbulence.

b. Results

Figure 3 shows maximum and minimum values within the model domain of the humidity with respect to water (RH) as functions of time. Initially, RH is 85%. It stays steadily at this value in case D, where we simulate an undisturbed atmosphere. However, in the other three cases where the atmosphere is perturbed by the aircraft vortices, the relative humidity field quickly (within about 1 min) produces maxima of more than 90%, that is, RH is more than 5% higher there than in the environment. In these regions of maximum relative humidity ice formation begins. The maximum RH changes little throughout the simulation. Simultaneously, the relative humidity field evolves a strong minimum that reaches about 67% or almost 20% less than the ambient value after 160 s in the three aircraft-affected cases. The time when the RH field reaches its first minimum is one quarter of the Brunt–Väisälä period when the initial downward motion of the vortices comes to rest. This shows that the RH minima are caused by the strong downward motion between the two counter-rotating vortices, which leads via adiabatic compression to higher temperature and lower humidity. Up to this time, the minimum humidity curves are congruent for cases A–C, which demonstrates the dominant role of the dynamics in this phase of the evolution. Later, at times $t \gtrsim 300$ s, the minimum curves separate showing the increasing importance of the different microphysical developments in the cloud. In this phase the condensation reduces the relative humidity down to ice saturation (in cases A and C) at RH $\approx$ 59%.

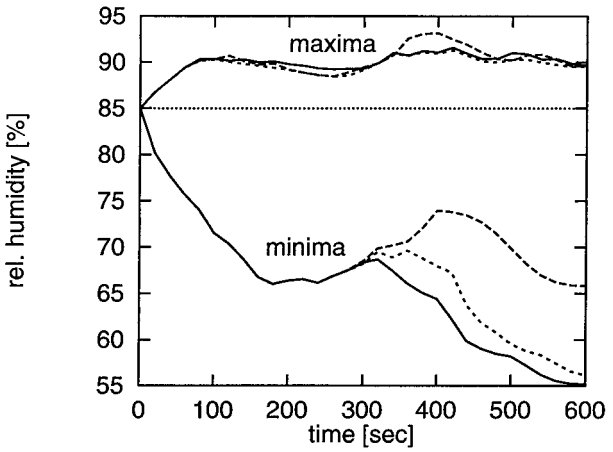

FIG. 3. Temporal evolution of maxima and minima in the relative humidity field for the cases A (solid), B (long dashed), C (short dashed), and D (dotted). In case D the atmosphere is not disturbed, thus the relative humidity stays constantly at its ambient value of 85%.

Now we consider in more detail the interaction between dynamics and microphysics for the most general case C, where both aerosol modes are present. For an overview, consider Fig. 4 that shows a time series of particle numbers, integrated over the model domain and per meter of flight path. We show the number of ice particles and the number of aerosol particles that contribute to the ice population. The total number of particles is not exactly conserved in the model. The error arises from the classic numerical problem of computing differences of large, nearly equal numbers. However, this error is two orders of magnitude smaller than the ice crystal number and may therefore be considered negligible. We see from Fig. 4 that during the first minute the ice particles form from nucleation of the large aerosol mode alone, the contribution of type A aerosol being very small. Both aerosol types contribute equally to the ice after about $t \approx 100$ s. The nucleation rate is very small from $t \approx 120$ until $t \approx 340$ s and the number of ice crystals stays almost constant. This time interval

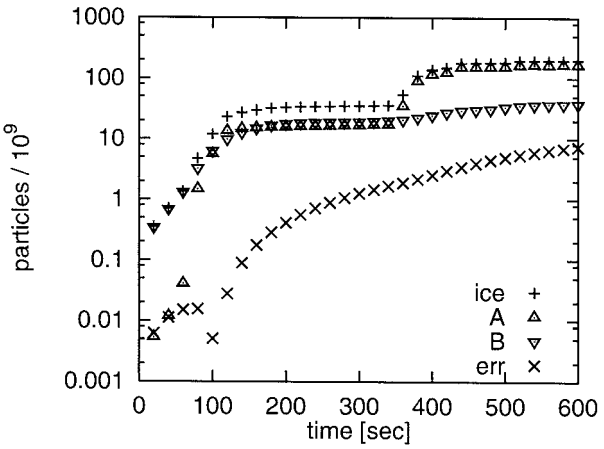

FIG. 4. Time series of particle numbers (in units of billions) integrated over the model domain and per meter of flight path for case C. Shown are the number of ice crystals (+) and the aerosol particles contributing to the ice population (A: △, B: ▽). The error (×) arises from violation of particle number conservation.

corresponds to the second quarter of the Brunt–Väisälä oscillation, when the downward motion between the two primary vortices comes to rest and two secondary vortices begin to develop. At $t \approx 360$ s, that is, at about half of the Brunt–Väisälä period, when the pair of secondary vortices begins to dredge up air from below the vortex system, the nucleation rate of aerosol type A increases (almost) suddenly (whereas type B seems to be only slightly affected) and the number of ice crystals increases in less than 1 min by almost an order of magnitude. After this short ''inflationary phase'' the nucleation is quenched and the number of ice crystals remains almost constant for the rest of the simulation.

Figure 5a shows the flow field at $t = 80$ s, that is, still in the first quarter of the Brunt–Väisälä period. One IWC contour is superposed, indicating an ice mass concentration of 0.01 mg m^{-3}. This ice is formed in the upper part of the vortex system where the relative humidity is enhanced due to adiabatic cooling in the upwelling limbs of the vortices. The ice is formed mainly by nucleation of the large aerosol type B. Locally, more than 50% of the type B particles are transformed into ice crystals. Figure 5b shows the corresponding situation at $t = 180$ s, that is, shortly after $T_{BV}/4$. Meanwhile, the new ice crystals have been mixed throughout the upper part of the vortex system. Although the relative humidity is reduced in the central downwash region, it is still above ice saturation. Hence the ice crystals grow by deposition. At the bottom edge of the vortex system the downwash is stopped abruptly, although the primary vortex is still present. The first signs of the development of the secondary vortex pair can be seen beneath the original vortex pair. Figure 5c shows the situation at $t = 360$ s, that is, at the beginning of the inflationary phase. The secondary vortex pair is now seen full in action as it dredges up air from below into the central region, thereby cooling it adiabatically and increasing its relative humidity. At the upper edge of this new moist bubble, where RH reaches values around 90%, the nucleation of aerosol type A furnishes a large number of new ice crystals. More than 10% of aerosol type A particles are transformed into ice locally. Although type B particles are depleted almost completely by nucleation at the same location, the contribution of the large aerosol mode to the new ice is masked by the nucleation of type A. (Remember that there are 500 times more particles of type A than of type B.) Figure 5d shows the final state of our simulation, that is, $t = 600$ s. The flow field is complex and nothing of the primary vortex pair is left. There is a large ice cloud with maximum ice concentrations exceeding 10 mg m^{-3}. The properties of this cloud will be considered next.

We have compiled microphysical and optical properties of the simulated clouds in Table 1. The entries for cases A, B, and C refer to the nonexhaust contrails, whereas those for case D refer to the thin cirrus deck that is forming at the upper boundary of the model domain. This cirrus deck is not yet old enough to be visible; with a maximum optical depth of 0.003 in the visual wavelength region, it is still far beneath the perception threshold ($\tau_{vis} \approx 0.02$). The optical depth has been determined diagnostically using the formula

$$\tau_\lambda = \int \mathrm{IWC}(a_\lambda + b_\lambda / r_{\mathrm{eff}})\, dz, \qquad (1)$$

with suitable constants a_λ and b_λ (Ebert and Curry 1992). The effective radius has been determined from the mean mass $\overline{m}$ of an ice crystal in a grid cell, assuming the mass–length relation for small column-shaped ice crystals of Starr and Cox (1985), an aspect ratio of 1:1, and a lognormal mass distribution (with a mode mass $m_{\mathrm{mode}} = 4\overline{m}$) of the ice crystals in a grid cell. The resulting formula is

$$\left(\frac{r_{\mathrm{eff}}}{\mu\mathrm{m}}\right) = 3.74 \times 10^5 \left(\frac{\overline{m}}{\mathrm{g}}\right)^{0.588} \left(\frac{m_{\mathrm{mode}}}{\overline{m}}\right)^{0.571}, \qquad (2)$$

where r_{eff} is in microns and $\overline{m}$ is in grams. The mean effective radius (averaged over the grid cells) of the ice crystals in the simulated wake induced ice clouds (A, B, and C) are similar to those given by Gayet et al. (1996) for the contrails they observed, although they use a formula for bullet rosettes. The effective radius is also similar in the simulated subvisible cirrus cloud of case D. The mean masses of the ice crystals are a few nanograms in all cases. The wake clouds (A–C) become visible ($\tau_{vis} > 0.02$) after about 60–100 s in the simulations, that is, during the first quarter of the Brunt–Väisälä period, when in Fig. 5a the first IWC contour (0.01 mg m^{-3}) appears. At the end of the simulations, that is, after 10 min of evolution, the optical depths in cases A and C are larger than usual for a contrail [a typical range being 0.1–0.8, although Schumann and Wendling (1990) reported a case with $\tau_{vis} > 1$]. The

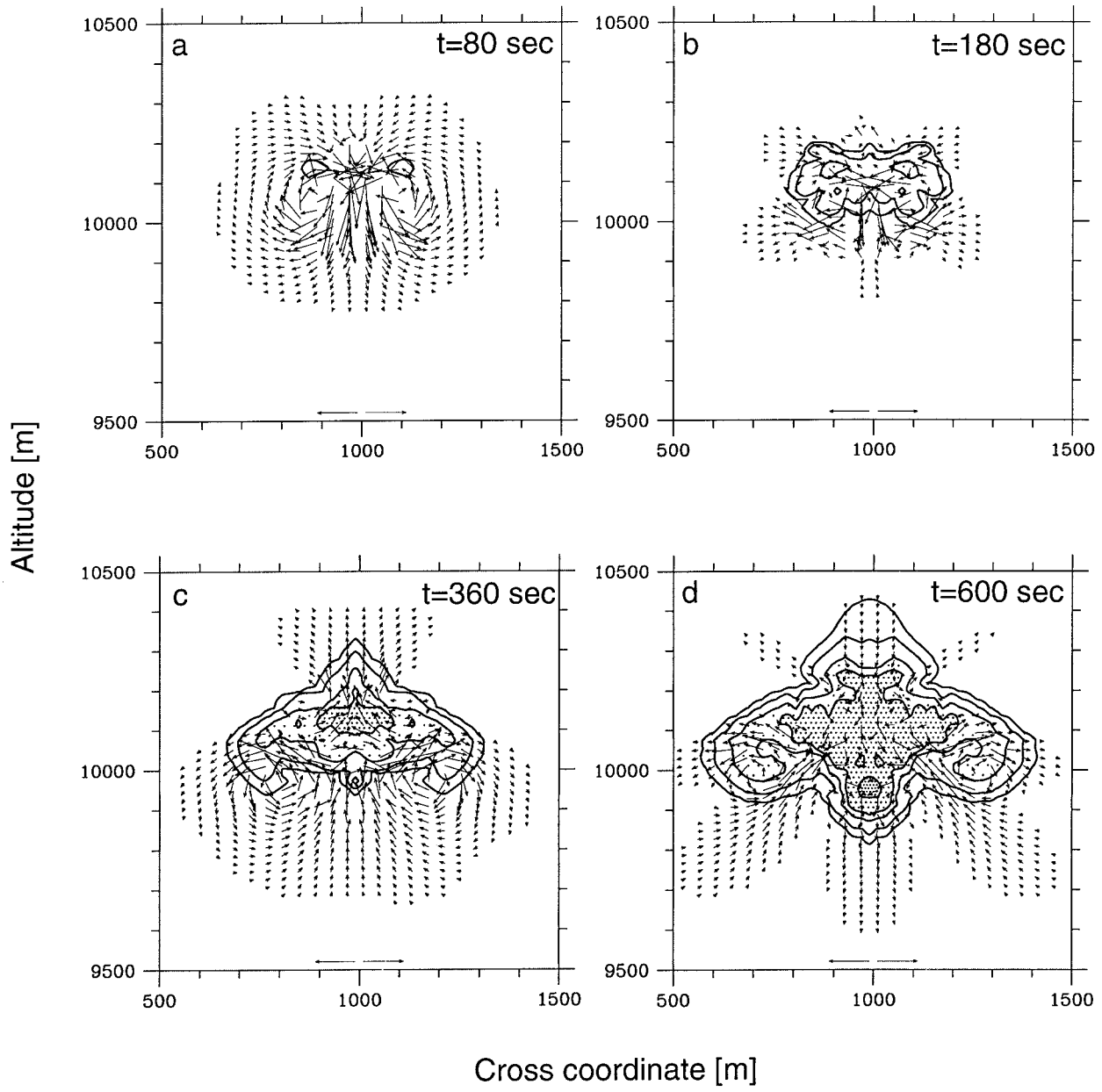

FIG. 5. Flow field and ice water concentration (contours and stipples) at four moments during the simulation of case C. Frame a: $t = 80$ s, b: $t = 180$ s, c: $t = 360$ s, d: $t = 600$ s. The IWC contours are 0.01, 0.1, 1.0 (low stipple density), 3. (medium), and 10 mg m^{-3} (high). The two arrows at the bottom of each frame indicate a velocity of 1 m s^{-1}.

high optical depths are caused by the high crystal concentrations that in these cases are one order of magnitude larger than those measured in contrails by Gayet et al. (1996). Only the case B cloud has properties (τ and $\langle \mathcal{N} \rangle$) that are similar to the contrails investigated by Gayet et al. Although it might be that Gayet et al. did hit the contrail edge rather than the center during their in situ measurement, it is more plausible to assume that the early nucleation of exhaust particles in a contrail reduces the humidity such that only big ambient aerosol particles have a chance to nucleate when they become lifted by the vortices. Small ambient aerosol particles would stay unactivated and form a contribution to the interstitial aerosol inside contrails. As expected, ice mass and crystal number concentrations are much lower in case D. In the altitude where the wake is situated in the other simulations, there is no ice at all. The total number of ice crystals is of the order 10^{11} m^{-1} in the wake clouds, which compares well with the numbers reported by Ström et al. (1994) for contrails. Mean and

TABLE 1. Microphysical and optical properties of simulated aerodynamically formed contrails after 10 min of integration time: average and maximum ice water content, total ice mass per meter of flight path average and maximum crystal number density, total number of ice crystals per meter of flight path, mean mass of ice crystals, mean effective radius, and maximum optical depths in the visual and infrared window spectral region. Note that the values given for case D refer to the cirrus deck that forms at the upper boundary of the computation domain.

Case	A	B	C	D
$\langle \text{IWC} \rangle$ [mg m^{-3}]	3.1	1.5	2.5	0.04
$\text{IWC}_{\max}$ [mg m^{-3}]	12.0	5.6	11.5	0.24
M_{tot} [kg m^{-1}]	0.592	0.297	0.530	0.042
$\langle \mathcal{N} \rangle$ [L^{-1}]	1666	188	912	5
$\mathcal{N}_{\max}$ [L^{-1}]	34 000	1000*	16 500	24
$\mathcal{N}_{\text{tot}}$ [10^{11} m^{-1}]	3.2	0.4	2.0	0.05
$\langle m \rangle$ [ng]	1.84	7.94	2.75	8.82
$\langle r_{\text{eff}} \rangle$ [μm]	13.5	15.3	13.8	13.5
$\tau_{\text{vis,max}}$	1.61	0.22	1.06	0.003
$\tau_{\text{win,max}}$	0.61	0.09	0.41	0.001

* Note that in this simulation all the available aerosols have nucleated locally.

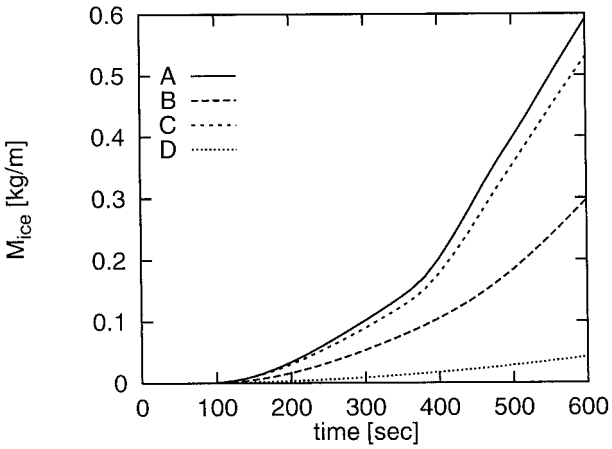

FIG. 6. Ice content within the aircraft wake induced ice clouds per meter of flight path (A, B, C) and in the subvisible cirrus deck (D) vs time.

maximum ice concentration in the wake clouds are similar to the corresponding properties of contrails (Gayet et al. 1996). This means that when the relative humidity is sufficiently high that the vortices can trigger nucleation of haze droplets, a significant fraction of the ice crystals found in contrails may originate from the nucleation of the ambient aerosol via aerodynamic effects.

Let us consider now the results in more detail. We find a maximum ice crystal concentration in case B of 1000 L^{-1}, which is identical to the ambient aerosol concentration. This means that at least locally all aerosol particles have been activated into ice. In case A, however, the maximum ice crystal number density is more than one order of magnitude less than the ambient aerosol concentration. This difference is due to the fact that large aerosol particles are more easily activated than small ones (the particles both being of the same chemical composition). In case C, where both aerosol populations are present, the ice crystal number densities are intermediate between those of cases A and B. Obviously, the nucleation and subsequent growth of the big (B) aerosol particles depletes the available water vapor, leaving the chance for a later nucleation of the small (A) aerosol particles significantly reduced. A population of preexisting ice crystals (subvisible cirrus) likely would decrease the peak water vapor saturation even more, resulting in less crystals nucleated, hence crystals could grow to precipitating sizes. Since they are less numerous, the ice crystals in case B can grow to larger sizes than those in case A. Case B ice crystals possess on the average more than four times the mass than the case A crystals. However, the sheer number of type A particles causes finally about twice as large an ice content (for the average and maximum values, see Table 1 and Fig. 6) in case A relative to case B. As before, the corresponding quantities in case C are intermediate between the case A and B values. Figure 6 shows that not only the ice content M_{ice} is larger in case A than in case B but also the ice production rate dM_{ice}/dt. Principally, a big crystal grows faster than a small one because of its larger surface area. This principle alone would imply a larger ice production rate in case B. However, many small crystals make up a larger total surface area than a few big ones. Then, the ensemble consisting of small crystals assumes the higher ice production rate. This explains why ice production proceeds faster in case A than in case B.

Because of the high ice supersaturation, the ice mass in the wake clouds grows rather fast (Fig. 6): after the 10 min of simulation time there is 0.592, 0.297, and 0.530 kg m^{-1} of ice in the cases A, B, and C, respectively. These amounts are of the same order of magnitude as the amounts of ice achieved after 30 min at a relative humidity of 70% (with respect to water) in the model contrails of Gierens (1996). Most of the wake cloud volume is still in an ice-supersaturated state after 10 min of simulation time. Thus, there is still a potential for further ice formation by deposition. Only in that region, where the secondary vortices cause the nucleation burst at about half of the Brunt–Väisälä period, is the humidity reduced to ice saturation and even below. If we define the cloud cross section via a crystal concentration threshold of at least 10 L^{-1}, we find inside of this boundary condensible masses of water vapor of 1.066, 1.381, and 1.268 kg m^{-1} for the cases A, B, and C, respectively. We see that the total amount of ice that can be produced in the wake of an aircraft by aerodynamic effects is similar to ice mass that is usually ascribed to the exhaust contrail. Both ways of ice production in an aircraft wake should be taken into account when in situ measurements of contrails are evaluated and interpreted.

4. Discussion

The results from this limited model study show the potential for ice cloud trails to form simply from aerodynamic effects caused by an aircraft. As for long lasting exhaust triggered contrails, the atmosphere must be at least saturated with respect to ice. The cases simulated in this study show two transitions occurring in the microphysical properties after about one quarter and one half the Brunt–Väisälä period, respectively. At both instances the crystal number concentration increases by roughly one order of magnitude. It is improbable that the second transition (the burst of nucleation of the small aerosol mode A induced by the secondary vortices) in reality appears with such clarity as in the simulation, because 1) the earlier nucleation of the exhaust aerosol reduces the available moisture and 2) atmospheric turbulence along with turbulence induced by the aircraft body erodes the vortices, so that they may not survive the first half of the Brunt–Väisälä period. However, the different formation locations of the two contrail types should make it possible to detect the aerodynamically formed one with a lidar system.

In the present simulation of wake-induced ice cloud formation we found a strong coupling between microphysics and vortex dynamics. On the contrary, it has been shown recently (Gierens 1996) that the microphysical evolution of exhaust triggered contrails depends primarily on ambient temperature and humidity and that dynamics does not have a strong influence. This difference can easily be explained by considering the different formation mechanisms of both types of clouds. Exhaust triggered contrails are formed early in the wake by activation of combustion products like soot (cf. Kärcher et al. 1996). Since (but for special circumstances) the water supersaturation reaches values of 200% and more in the early wake, a large fraction (if not all) exhaust soot particles are activated to droplets that may freeze afterwards. This process is so rapid that it cannot be coupled to the vortex dynamics. Once the contrail is formed, its evolution is controlled by diffusional growth and evaporation of the ice crystals, which in turn is controlled primarily by ambient temperature and ice supersaturation. On the other hand, the vortex field behind an aircraft is essential for the formation of an aerodynamically induced trail: It is the lifting of moist ambient aerosol laden air above the nucleation threshold that initiates the formation of this type of ice cloud.

In this study the ambient aerosol was assumed to consist of ammonium sulfate only, because this allowed us to employ the nucleation parametrization by DeMott et al. (1994). Ammonium sulfate is commonly used in models for low-level clouds; however, in the upper troposphere it is conceivable that the sulfate aerosol is less neutralized and composed in higher proportions of sulfuric acid and ammoniumbisulfate particles. This difference in chemical composition may be of great importance for the detailed microphysical properties of natural cirrus clouds where the cooling rates are much smaller than in the wake of the simulated contrails. At the deliquescent point for ammonium sulfate (82%), the ice nucleation rate is very low due to the solution droplets being highly concentrated, which would be true for other sulfates as well. A relative humidity of 82% with respect to water is equivalent to 139% with respect to ice at -56°C. Due to the strong nonlinearity in the ice nucleation rate as a function of humidity the turbulence from an aircraft may be all that is needed to drive the atmosphere out of this metastable state to approach the equilibrium state, or ice saturation. That such metastable states with highly ice-supersaturated regions in clear air exist is known from FIRE-II aircraft measurements (Heymsfield and Miloshevich 1995). However, it is difficult to estimate the spatial and temporal extents of such metastable conditions, since humidity data for the upper troposphere are known to have large uncertainties. Regardless of the chemical or physical nature of the ambient aerosol, ice saturation must at least be reached in the ambient air in order for the contrails to be persistent.

An exhaust contrail forms during the early jet phase of the wake (i.e., <1 s plume age). In this phase, the vortices are in a nascent state, hence the interaction between the exhaust jet and the vortices is weak. Consequently, the vortex dynamics does not appear in Appleman's theory that formulates the conditions of exhaust contrail formation. Obviously, the formation of an aerodynamically triggered wake cloud is logically disconnected from the Appleman criterion. Therefore, it is possible *in principle* that such a wake cloud appears in situations when the Appleman criterion is not fulfilled and no exhaust contrail forms. However, it seems very improbable that such a situation really occurs since the nucleation process that leads to aerodynamic contrail formation is strongly dependent upon ambient temperature and humidity. At temperatures above the Appleman threshold it could be that all conceivable nucleation processes proceed too slowly for making a noticeable effect.

Finally we discuss which aircraft parameters influence the formation of wake clouds. There are four independent parameters that characterize the dynamics of an aircraft and its wake. These are weight W, speed V, wing span B, and wing area A or lift coefficient c_L ($c_L = 2W/A\rho V^2$ with air density ρ). Since the vortices that cause the effect are shed from the trailing edges of the wings and are not much affected by the wing surface, we assume that the wing area is not important for the formation and strength of the wake clouds. On the other hand, it is reasonable to assume that the mass that is contained in the vortex system is an important factor that determines how much ice can be formed in the wake by aerodynamic effects. This mass (per unit length of

flight path) is proportional to the square of the wing span:

$$M = (\pi^3/8)\rho B^2. \quad (3)$$

Secondly, we assume that the effect is the stronger the faster the air is lifted in the vortex system. This speed can be measured in terms of the circulation Γ of each vortex, which Γ is related to the aircraft parameters in the following way:

$$\Gamma = \frac{4}{\pi\rho}\frac{W}{V}\frac{1}{B}. \quad (4)$$

We see that Γ is inversely proportional to the wing span B and directly proportional to the ratio W/V, which is the momentum released to the air by the aircraft per unit length of flight path. This quantity can also be expressed using the velocity U of the downward traveling vortex pair: $W/V = MU$. From this discussion we may conclude that the ice formation in the wake grows with wingspan B and momentum release rate W/V. In order to test these assumptions we have performed two additional simulations, one with half the initial vortex area (representing smaller span B) compared to the reference case C and another one with an initial value of $U = 1.8$ m s^{-1} instead of 2.5 m s^{-1} (representing smaller W/V). As expected, in both cases we got lower crystal number concentrations and IWC than in the reference case C. The resulting total ice masses after 10 min of evolution were significantly smaller than in case C: in the case with reduced W/V the resulting ice mass was 0.327 kg m^{-1}, which means a 40% reduction, and in the case with reduced span B the ice mass came out with 0.224 kg m^{-1}, that is, almost 60% less than in case C. We see that aerodynamic ice cloud formation is strong for a heavy, slow, wide-body aircraft and vice versa.

5. Summary

In the present paper we have performed simulations of aerodynamically induced ice cloud formation in the wake of an aircraft flying at cruise altitude (10 km). In the up-welling limbs of the vortex pair behind an aircraft the lifted air is cooled adiabatically. This leads to a sharp increase in the freezing rate of the ambient haze droplets so that a cloud may form at the upper edge of the vortex system. In order to simplify the interpretation of the results we have excluded the exhaust particles from the simulation and assumed a calm atmosphere without background turbulence. Unlike a contrail that is formed by activation of exhaust particles, the evolution of an aerodynamically induced contrail depends on dynamic properties of the wake and the ambient atmosphere. It should be detectable with a lidar system. Conceivably an ice cloud can be induced in the wake of an aircraft when, according to the Appleman criterion, an exhaust triggered contrail would not form. However, such situations are certainly rather rare. The ice mass in a wake-induced ice cloud increases with the momentum the triggering aircraft releases on the ambient air and with the wing span. We find that aerodynamically induced ice clouds are similar in microphysical (IWC, crystal concentration, total ice mass, and crystal number) and radiative respects (visual optical thickness) to contrails that are formed from the nucleation of exhaust particles. This means that under cold and moist conditions contrails may consist of similar amounts of aerodynamically produced and exhaust triggered ice crystals. This should be taken into account when in situ measurements of contrails are evaluated.

Acknowledgments. The authors thank T. Gerz for fruitful comments. The work has been funded by the Commission of the European Union via the project AEROCONTRAIL (Contract ENV4-CT95-0157) and support by NFR (Swedish Natural Science Research Council).

APPENDIX

Numerical Representation of Ice Formation

We assume that the sizes r (spherical dry solute radius) of the aerosol particles (types A and B) obey a lognormal distribution law, that is,

$$n(r) = (\sqrt{2\pi}r\ \ln\sigma)^{-1}\ \exp[-\ln^2(r/r_g)/2\ \ln^2\sigma]. \quad (A1)$$

According to DeMott et al. (1994), the fraction F_{hf} of haze particles, containing given masses $m_s = (4\pi/3)\rho_s r^3$ of dry aerosol that nucleate within a time step Δt, can be written as

$$F_{hf}(r) = 1 - \exp[-a(2r)^6\Delta t], \quad (A2)$$

where the factor a depends on relative humidity, temperature, and aerosol properties. If we write N_t for the total number of haze particles, then the number of haze particles that freeze homogeneously in time Δt is

$$N_f = N_t \int_0^\infty F_{hf}(r)n(r)\ dr = N_t I. \quad (A3)$$

Now we substitute x for $\ln(r/r_g)/\sqrt{2}\ \ln\sigma$, so that the integral I can be written as

$$I = \frac{1}{\sqrt{\pi}}\int_{-\infty}^{\infty}\langle 1 - \exp\{-a\ \exp[6(\sqrt{2}\ \ln\sigma x + \ln r_g)]\Delta t\}\rangle e^{-x^2}\ dx. \quad (A4)$$

Written in this form, the integral can be evaluated by a Gauss–Hermite quadrature formula with weights w_i and abscissas x_i (see Abramowitz and Stegun, 1965):

$$I = \frac{1}{\sqrt{\pi}} \sum_{i=-i_m}^{i=+i_m} w_i \langle 1 - \exp\{-a \exp[6(\sqrt{2}\ln\sigma x_i + \ln r_g)]\Delta t\}\rangle. \quad \text{(A5)}$$

We use a 10-point ($i_m = 5$) quadrature formula in our code.

The mass of newly formed ice is determined as follows: The equilibrium size R of a haze particle or solution droplet at saturation ratio S is given implicitly by the Köhler equation, which in its simplest form can be written as

$$S(R) = 1 + A/R - B/R^3, \quad \text{(A6)}$$

where $A = A(T)$ is a function of temperature and $B = B(m_s)$ depends in particular on the mass of solute in the droplet. Along with DeMott et al. we assume that the solute is pure ammonium sulfate. The Köhler equation in its form given above can be inverted analytically, which explicitly gives the equilibrium radius R of the haze particle as a function of saturation ratio S and dry aerosol mass m_s (via B).

Let $\delta S = \sqrt{4A^3/27B}$ be the critical supersaturation of the Köhler theory, that is droplets can grow without limit for $S > 1 + \delta S$. Then we have to distinguish three cases:

Case 1) $S < 1 - \delta S$:

$$R(S) = \frac{2A}{3(1 - S)}[\cosh(\varphi/3) - 1], \quad \text{(A7)}$$

where

$$\varphi = \operatorname{acosh}\left[2\left(\frac{1 - S}{\delta S}\right)^2 - 1\right]; \quad \text{(A8)}$$

case 2) $1 - \delta S < S < 1$:

$$R(S) = \frac{2A}{3(1 - S)}[\cos(\psi/3) - 1], \quad \text{(A9)}$$

where

$$\psi = \arccos\left[\left|1 - 2\left(\frac{1 - S}{\delta S}\right)^2\right|\right]. \quad \text{(A10)}$$

At the special value $S = 1 - \delta S$ we get $R = \sqrt{3B/4A}$; and

case 3) $1 < S < 1 + \delta S$:

$$R(S) = \sqrt{3B/4A}[\cos(\chi/3)]^{-1}, \quad \text{(A11)}$$

where

$$\chi = \arccos\left(\frac{1 - S}{\delta S}\right). \quad \text{(A12)}$$

Special values are $R(S = 1) = \sqrt{B/A}$ and $R(S = 1 + \delta S) = \sqrt{3B/A}$.

The mass of the freezing solution droplet or haze particle is then $M = (4\pi/3)\rho_w R^3$ with the water density ρ_w.

REFERENCES

Abramowitz, M., and I. A. Stegun, 1965: *Handbook of Mathematical Functions.* Dover Publications, 1046 pp.

Appleman, H., 1953: The formation of exhaust condensation trails by jet aircraft. *Bull. Amer. Meteor. Soc.,* **34,** 14–20.

DeMott, P. J., M. P. Meyers, and W. R. Cotton, 1994: Parameterization and impact of ice initiation processes relevant to numerical model simulations of cirrus clouds. *J. Atmos. Sci.,* **51,** 77–90.

Ebert, E. E., and J. A. Curry, 1992: A parameterization of ice cloud optical properties for climate models. *J. Geophys. Res.,* **97,** 3831–3836.

Foster, T. C., and J. Hallett, 1993: Ice crystals produced by expansion: Experiment and application to aircraft-produced ice. *J. Appl. Meteor.,* **32,** 716–728.

Gayet, J. F., G. Febvre, G. Brogniez, H. Chepfer, W. Renger, and P. Wendling, 1996: Microphysical and optical properties of cirrus and contrails: Cloud field study on 13 October 1989. *J. Atmos. Sci.,* **53,** 126–138.

Gierens, K. M., 1996: Numerical simulations of persistent contrails. *J. Atmos. Sci.,* **53,** 3333–3348.

Heymsfield, A. J., and L. M. Miloshevich, 1993: Homogeneous ice nucleation and supercooled liquid water in orographic wave clouds. *J. Atmos. Sci.,* **50,** 2335–2353.

——, and ——, 1995: Relative humidity and temperature influences on cirrus formation and evolution: Observations from wave clouds and FIRE II. *J. Atmos. Sci.,* **52,** 4302–4326.

Höller, H., 1986: Parameterization of cloud-microphysical processes in a three-dimensional convective mesoscale model. DFVLR Forschungsbericht 86-02, 82 pp. [Available from Deutsche Forschungsanstalt für Luft- und Raumfahrt, D-51140 Köln, Germany.]

Kajikawa, M., and A. J. Heymsfield, 1989: Aggregation of ice crystals in cirrus. *J. Atmos. Sci.,* **46,** 3108–3121.

Kärcher, B., T. Peter, U. M. Biermann, and U. Schumann, 1996: The initial composition of jet condensation trails. *J. Atmos. Sci.,* **53,** 3066–3083.

Knollenberg, R. G., 1972: Measurements of the growth of the ice budget in a persisting contrail. *J. Atmos. Sci.,* **29,** 1367–1374.

Koenig, L. R., 1971: Numerical modelling of ice deposition. *J. Atmos. Sci.,* **28,** 226–237.

Lin, H., K. J. Noone, J. Ström, and A. J. Heymsfield, 1998: Small ice crystals in cirrus clouds: A model study and comparison with in situ observations. *J. Atmos. Sci.,* **55,** 1928–1939.

Noone, K. J., J. A. Ogren, J. Heintzenberg, R. J. Charlson, and D. S. Covert, 1988: Design and calibration of a counterflow virtual

impactor for sampling of atmospheric fog and cloud droplets. *Aerosol Sci. Technol.*, **8,** 235–244.

Ponater, M., S. Brinkop, R. Sausen, and U. Schumann, 1996: Simulating the global atmospheric response to aircraft water vapour emissions and contrails—a first approach using a GCM. *Ann. Geophys.*, **14,** 941–960.

Rangno, A. L., and P. V. Hobbs, 1983: Production of ice particles in clouds due to aircraft penetration. *J. Climate Appl. Meteor.*, **22,** 214–232.

Rogers, R. R., 1979: *A Short Course in Cloud Physics.* 2d ed. Pergamon Press, 235 pp.

Sassen, K., 1991: Aircraft-produced ice particles in a highly supercooled altocumulus cloud. *J. Appl. Meteor.*, **30,** 765–775.

——, and G. C. Dodd, 1989: Haze particle nucleation simulation in cirrus clouds and applications for numerical and lidar studies. *J. Atmos. Sci.*, **46,** 3005–3014.

Schumann, U., 1996: On conditions for contrail formation from aircraft exhausts. *Meteor. Z., N. F.*, **5,** 4–23.

——, and P. Wendling, 1990: Determination of contrails from satellite data and observational results. *Air Traffic and the Environment,* U. Schumann, Ed., Springer-Verlag, 138–153.

——, T. Hauf, H. Höller, H. Schmidt, and H. Volkert, 1987: A mesoscale model for simulation of turbulence, clouds and flow over mountains: Formulation and validation examples. *Beitr. Phys. Atmos.*, **60,** 413–446.

Starr, D. O., and S. Cox, 1985: Cirrus clouds. Part I: A cirrus cloud model. *J. Atmos. Sci.*, **42,** 2663–2681.

Stephens, G. L., S. Tsay, P. W. Stackhouse, and P. J. Flatau, 1990: The relevance of the microphysical and radiative properties of cirrus clouds to climate and climatic feedback. *J. Atmos. Sci.*, **47,** 1742–1753.

Ström, J., F. Schröder, J. Heintzenberg, T. Anderson, P. Wendling, and B. Strauss, 1994: Recent measurements in cirrus clouds and contrails using the MISU CVI-payload during ICE94. *7th EUCREX-2 Workshop,* Lille, France, Université des Sciences et Technologies de Lille, 83–85. [Available from Dr. J. Ström, Dept. of Meteorology, Stockholm University, S-10691 Stockholm, Sweden.]

——, B. Strauss, T. Anderson, F. Schröder, J. Heintzenberg, and P. Wendling, 1997: In situ observations of the microphysical properties of young cirrus clouds. *J. Atmos. Sci.*, **54,** 2542–2553.